Electronic Supplementary Material (ESI) for CrystEngComm.

# Electronic Supplementary Information

*for*

## 10-vertex closo-carborane: a unique ligand platform for porous coordination polymers

*by*

**Ishtvan Boldog,*[a,b] Pablo J. Bereciartua,[c] Roman Bulánek,[d] Monika Kučeráková,[c] Markéta Tomandlová,[a] Michal Dušek,[c] Dirk De Vos*[b] and Tomáš Baše*[a]**

[a] *Institute of Inorganic Chemistry, The Czech Academy of Sciences, v.v.i. 250 68 Husinec-Řež, č.p. 1001, Czech Republic. E-mail: ishtvan.boldog@gmail.com, tbase@iic.cas.cz*

[b] *Faculty of Bioscience Engineering, Department of Microbial and Molecular Systems, Centre for Surface Chemistry and Catalysis, KU Leuven, Celestijnenlaan 200F, postbox 2461, 3001 Leuven, Belgium. E-mail: dirk.devos@biw.kuleuven.be*

[c] *Institute of Physics, The Czech Academy of Sciences, Na Slovance 2, 182 21 Prague 8, Czech Republic*

[d] *Department of Physical Chemistry, Faculty of Chemical Technology, University of Pardubice, 532 10 Pardubice, Czech Republic*

# TABLE OF CONTENTS

## *Synthesis of 1,10-dicarboxy-1,10-dicarba-*closo*-decaborane ($H_2L$)*

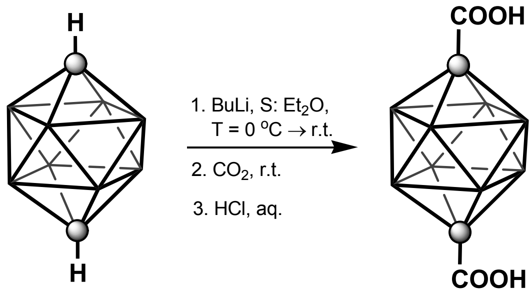

**SFig. 1.** Synthesis of $H_2L$.

$H_2L$ was synthesized via a standard sequence (SFig. 1) for functionalization of carboranes, namely lithiation and carbonylation according to *Zakharkin et. al.*[1] (see also [2]).

To a stirred slurry of 1220 mg (10 mmol) of 1,10-dicarba-*closo*-decaborane (Katchem) in 150 ml of $Et_2O$ freshly distilled from a sodium benzophenone ketyl solution, 8.8 ml (22 mmol ) of 2.5 M butyl lithium solution in hexane (Aldrich) was added during 2 minutes in small portions under stirring at 0-5°C (ice / water bath) in argon atmosphere. A white precipitate of the lithiated product started to precipitate in a short time. The slurry was allowed to heat-up to room temperature and after 1h of stirring $CO_2$ gas, generated by evaporation of dry-ice, was bubbled through the solution (3-5 L/h) during ~6h (Caution! The exhaust stream of $CO_2$ contain vapours of ether and non-desired concentration of vapors should be considered in the context of safety. Work in a fumehood is advised. The precipitation of the lithium salt of the carboxylated carborane started almost immediately after the bubbling started and the reaction seems to be mostly finished within 1h).

The ethereal solution was evaporated to dryness and the residue was quenched with 100 ml of water with a formation of almost clear solution and acidified by 10% aqueous HCl until pH~2. The formed precipitate was filtered-off, washed with water (3 × 10 ml). After drying in air the crude product (1755 mg) was sublimed (100-130°C, 0.05-0.1 Torr), yielding 1420 mg (68%) of white solid.

$H_2L$ is only very slightly soluble in water and ether, has appreciable solubility in alcohols and very well soluble in DMF and DMSO.

NMR spectra of $H_2L$ were measured on a Varian Mercury Plus 400 NMR spectrometer under standard conditions on freshly prepared samples, using deuterated acetone as solvent. $^{11}B$ chemical shifts are given relative to $BF_3 \cdot OEt_2$, and $^{1}H$ and $^{13}C$ chemical shifts relative to TMS. The reference frequencies were estimated based on the frequency of the lock signal as a secondary standard. $^{1}H$ NMR ($CDCl_3$, 400 MHz; $^{11}B$ decoupled): $\delta = 2.44$ (s, 8H;); $^{11}B$ NMR ($CDCl_3$,128 MHz; $^{1}H$ decoupled) $\delta = -10.89$ (s, 8B); $^{13}C$ NMR ($CDCl_3$, 100 MHz): $\delta = 118.4$ ($C\mathbf{C}B_4$), 165.1 ($O_2\mathbf{C}C$); the ordinary and decoupled spectra are given on SFig. 2-4. M.p.: 303-304 °C, measured in

---

[1] L. I. Zakharkin and A. I. Kovredov, *Zhurnal Obshchei Khimii* 1974, **44**, 1840-1841.

[2] P. M. Garrett, J. C. Smart and M. F. Hawthorne, *J. Am. Chem. Soc.* 1969, **91**, 4707-4710.

a sealed glass capillary. The compound turned brownish near melting point, and the degradation, observed as darkening, accelerated with further increase of temperature.

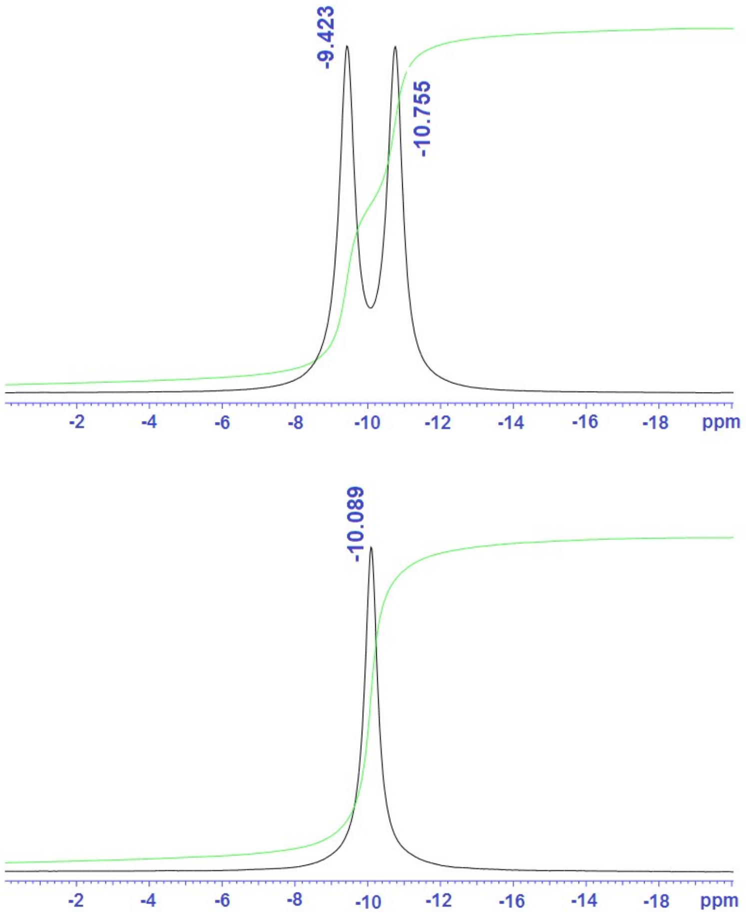

**SFig. 2.** $^1H$ coupled and decoupled $^{11}B$ NMR spectra of $H_2L$

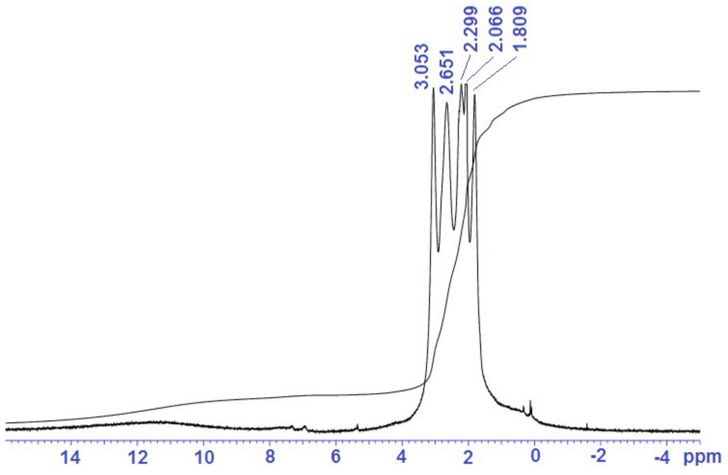

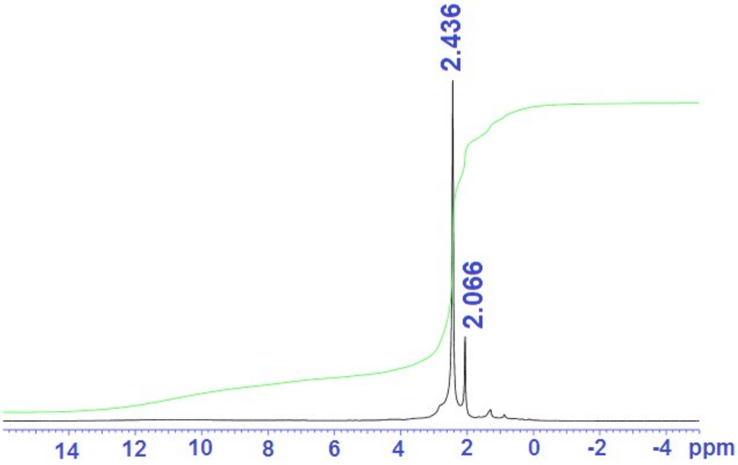

**SFig. 3.** $^{11}B$ coupled and decoupled $^{1}H$ NMR spectra of $H_2L$

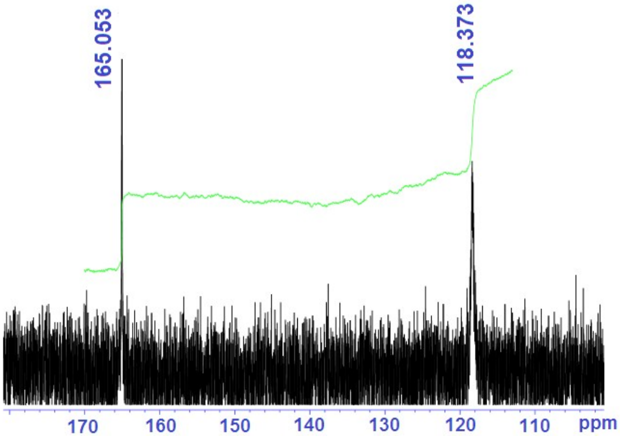

**SFig. 4.** $^{13}C$ NMR spectrum of $H_2L$

## *Syntheses of the porous coordination polymers (PCPs)*

**Materials and methods.** $Co(NO_3)_2 \cdot 6H_2O$ (98%, Lachema Brno), $Cu(NO_3)_2 \cdot 3\,H_2O$ (98%, Alfa Aesar), $Zn(NO_3)_2 \cdot 6H_2O$ (99%, Sigma Aldrich), N,N-dimethylformamide (99.8%, Sigma Aldrich), N,N-diethylformamide (99%, Sigma Aldrich), $HNO_3$ (63% aq. sol., reagent grade), EtOH (95%, Penta). The syntheses of PCPs given below were reproduced on larger (~×3-5) scales.

### Synthesis of $[Zn_4OL_3(DEF)_3]$, 1

A solution of 43 mg (0.145 mmol) of zink nitrate hexahydrate and 20 mg (0.096 mmol) of $H_2L$ in 2ml of $1{:}1_{vol}$ DEF/EtOH$_{96\%}$ was sealed in 4 ml screw-cap vial and heated at 90°C for 3 days (DEF = N,N-diethylformamide). Within the first 12h long (up to 2 mm length) flat-needles was growing chiefly (the optimal temperature of formation is somewhat lower, 70-80°C), which were futher redissolved / converted to an other phase, consists of transparent 'tabular' blocks (diameter up to 0.7 mm).

After cooling, the solvent was syringed out, the crystals were washed by a small amount of DEF and dried ($5 \cdot 10^{-2}$ Torr, RT, 2h), the yield of the colorless crystals was 31 mg (80%, ligand based) (all operations were performed avoiding contact with air and the product was stored under argon).

### Synthesis of [Co(DMF)L], 2

A solution of 56 mg (0.192 mmol) of cobalt nitrate hexahydrate and 20 mg (0.096 mmol) of $H_2L$ in 2ml of 1:1 DMF / EtOH (96%) mixture was sealed in a 4 ml screw-cap vial and heated at 85°C for 3 days yielding aggregates of elongated tapering blocks (up to 0.3 mm length) of red color (DMF = N,N-dimethylformamide). The yield of the red crystalline product after removing the solvent, washing with a small amount of DMF and drying ($5 \cdot 10^{-2}$ Torr, RT, 2h) was 23 mg (80%, ligand based).

### Synthesis of $[Cu_2L_2(DMF)_2] \cdot 2\,DMF$, 3

A solution of 300mg (1.25 mmol) of $Cu(NO_3)_2 \cdot 3H_2O$ and 180 mg of $H_2L$ (0.86 mmol) was placed in a 20 ml glass vial and dissolved in 18 ml of DMF after prolonged shaking. To the formed blue solution 180 μL of conc. $HNO_3$ (~60%) were added at once and immediately homogenized (practically no color change was observed).

The sealed vial was heated in an oven at 70°C for 8 days. The crystallization started in 3 days and finally resulted in large (up to 1 mm) blue right square prismatic crystals, close to cubes. The yield after removing the solvent, washing with a small amount of DMF and drying under reduced pressure ($5 \cdot 10^{-2}$ Torr, RT, 2h) was approx. 120 mg (33%, ligand based).

The crystallization of this compound on smaller scale proceeds faster and is mostly finished in 3-4 days at 1/10-th of the given scale. Heating times exceeding one week invoked a significant risk of contamination of the product with copper (I) oxide, the formation of which was sometimes observed in repeated experiments.

The same crystallization conditions, but without nitric acid as well as change the solven to DEF or mixtures with addition of ethyl alcohol lead to a poorly defined, but crystalline precipitate consists of small green or greenish-blue platelets, stacked in columns.

# *Additional notes upon single crystal XRD structures*

## Experimental details

Selected single crystals of suitable optical quality coated in perfluorinated oil or epoxy glue were mounted on a capton loop or glass fiber, transferred to an Agilent Gemini diffractometer equipped with a mirror-monochromated Cu X-ray source (Cu-Ultrs) and CCD detector Atlas, and measured at low or room temperature under protective dinitrogen gas stream controlled by a Cryojet system. Room temperature measurements proved to be better for **2** and **3**: cooling proved to be detrimental, possibly due to commencing phase-transition.

Data reduction and empirical absorption correction using spherical harmonics (Scale3 Abspack scaling algorithm) was performed by CrysAlis PRO software (Agilent, 2010). Lattice parameters initially determined for a limited reflection set were later refined against all data.
The structures were solved by direct methods (Burla, SIR-92)[1] or charge flipping (Superflip)[2] and refined using Jana2006 program (**1** and **2** on $F^2$ and **3** on $|F|$).[3] Non-hydrogen atoms were refined anisotropically and the disorder of the solvent molecules was thoroughly modelled using restraits of bond lengths and thermal displacement parameters), with the exception $[Cu_2L_2(DMF)_2] \cdot 2$ DMF, where the objective limitations of crystal quality prevented the refinement of all structural features. An important feature of the structure of $[Zn_4OL_3(DEF)_3]$ is the rotational disorder of the carborane moieties, which was treated by rigid body restraints.

Hydrogen atoms attached to carbon were placed on idealized positions. Positions of hydrogen atoms of the carborane moieties were refined for **1** and **2**, while in case of **3** they were fixed geometrically due to data quality. The ADP parameters of hydrogen atoms were in all cases derived from their parent atoms: $U_{iso}(H) = 1.2*U_{eq}(X_{parent})$, X = C, B.

The relatively high R-indices for $[Cu_2L_2(DMF)_2] \cdot 2$ DMF is objectively determined by the quality of the crystals: a number of them were tried without being successful in getting single crystals of high quality regarding diffraction.

Molecular graphics was prepared using DIAMOND software [4].

## Crystal data and structure refinement parameters

**Table S1.** Crystal data and structure refinement for $[Zn_4OL_3(DEF)_3]$, **1**; [Co(DMF)L], **2**; $[Cu_2L_2(DMF)_2] \cdot 2$ DMF, **3**.

| | **1** | **2** | **3** |
|---|---|---|---|
| Empirical formula [a)] | $C_{27.5}H_{58.1}B_{24}N_{3.1}O_{16.1}Zn_4$ | $C_{14}H_{30}B_{16}Co_2N_2O_{10}$ | $C_{11}H_{16}B_{16}O_{11.4}Cu_2$ |
| $M_r$ /g mol$^{-1}$ | 1211.1 | 677.2 | 630.7 |
| $T$ /K | 150 | 300 | 300 |
| Wavelength / Å [b)] | 1.5418 | 1.5418 | 1.5418 |
| Crystal system | orthorhombic | monoclinic | tetragonal |
| Space group | *Pna2₁* | *C2/c* | *I4₁md* |

---

[1] Burla M.C., Cascarano G. and Giacovazzo C., Acta Cryst., **1992**, A48, 906-912.

[2] Palatinus L., Chapuis G., J. Appl. Cryst., **2007**, 40, 786-790.

[3] V. Petříček, M. Dušek, L. Z. Palatinus, *Kristallogr.* **2014**, *229*, 345-352.

[4] K. Brandenburg, Diamond (Version 3.2g), Crystal and Molecular Structure Visualization, Crystal Impact – K. Brandenburg & H. Putz, Bonn (Germany) (**1997-2011**).

| | | | |
|---|---|---|---|
| $a$ /Å | 20.8189(4) | 14.3465(7) | 31.1622(12) |
| $b$ /Å | 23.3745(5) | 22.4400(11) | 31.1622(12) |
| $c$ /Å | 12.7036(3) | 19.3715(11) | 11.1615(5) |
| $\beta$ /° | 90 | 92.822(4) | 90 |
| $V$ /Å$^3$ | 6182 | 6228.8(6) | 10838.7(8) |
| Z | 4 | 8 | 8 |
| Calc. density /g cm$^{-3}$ | 1.301 | 1.440 | 0.773 |
| µ / mm$^{-1}$ | 2.206 | 8.75 | 1.19 |
| F(000) | 2455 | 2736 | 2490 |
| Crystal size /mm$^3$ | 0.175 × 0.141 × 0.105 | 0.159 × 0.098 × 0.043 | 0.25 × 0.23 × 0.22 |
| θ range /° | 3.7 - 67.1 | 3.6 - 66.5 | 2.8 - 67.0 |
| Index ranges /*hkl* | [-24, 24]; [-27, 26]; [-12, 14] | [-16, 16]; [-26, 26]; [-22, 22] | [-37, 26]; [-36, 22]; [-12, 13] |
| Reflections collected (R$_{int}$) | 39972 (0.0326) | 39599 (0.07) | 14479 (0.040) |
| Independent reflections | 9754 | 18483 | 4752 |
| Completeness /% to θ /° | 99% to 67.09 | 98% to 66.5 | 98% to 65.82 |
| Absorption correction | multi-scan | multi-scan | multi-scan |
| Max. and min. transmission | 0.712 and 1 | 0.336 and 1 | 0.692 and 1 |
| Data / restraints / parameters | 9754 / 27 / 454 | 23222 / 7 /312 | 4752 / 0 /203 |
| Goodness-of-fit [c)] | 2.65 | 2.22 | 4.16 |
| $R1$, $wR2$ [I>2σ(I)] | 0.0617, 0.1634 | 0.081, 0.196 | 0.093, 0.192 |
| $R1$, $wR2$ (all data) | 0.0669, 0.1675 | 0.139, 0.206 | 0.105, 0.195 |
| Largest diff. peak and hole, eÅ$^{-3}$ | 2.91 and -1.89 | 0.81 and -0.70 | 0.93 and -0.68 |

[a)] The compositions are given with fractional atom counts due to partial occupation of the guest molecules in **1** and **3** .

[b)] Agilent Xcalibur four-cycle diffractometer, Atlas detector, Gemini ultra

[c)] The Jana2006 program uses other approach for calculation of the goodness of fit compared to SHELXL, namely it does not refine the weighing scheme and uses weights from the experiment. Thus, increased GOF reflects either not fully solved disordered or complicated structures, or bonding effects revealed by very good data but undescribed with the standard crystallographic model.

## $[Zn_4OL_3(DEF)_3]$, 1

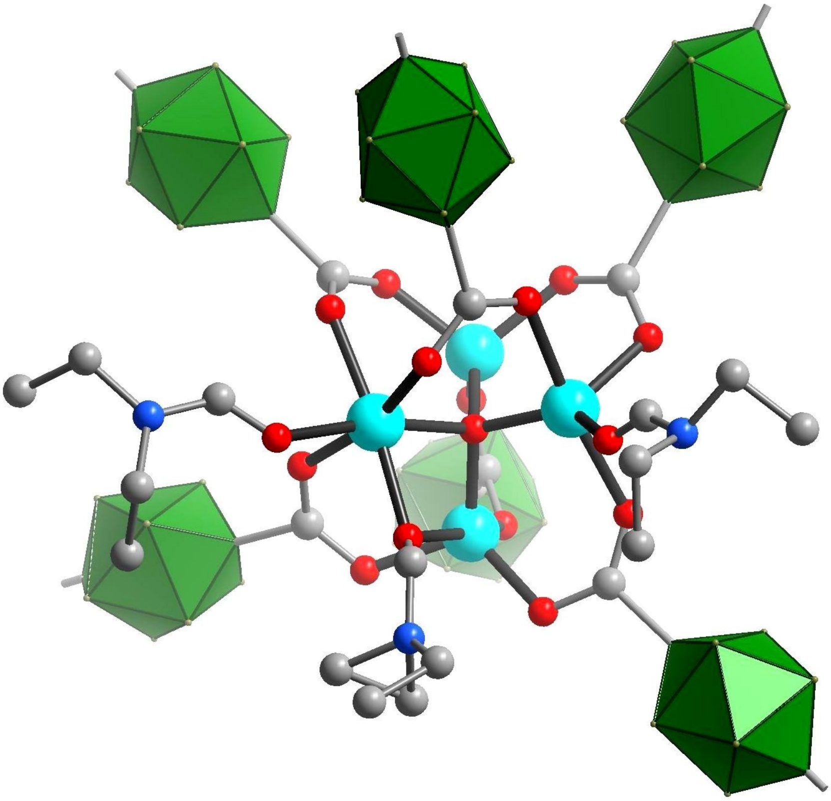

**SFig. 5.** The coordination bonded zinc cluster in $[Zn_4OL_3(DEF)_3]$ with the coordinated solvent molecules shown (the coordination bonds are accentuated). Note the dissymmetry of the coordination environment:

- the disordered DEF molecules coordinates only to 3 out of the 4 zinc ions, with one molecule fulfilling a bridging function.
- one out of the six bridging carboxylates (top, center on the image) is especially strongly deflecting from the idealized orientation (R-C bonding directions in idealized $\{Zn_4O(R\text{-}COO)_6\}$ cluster have an octahedral symmetry).

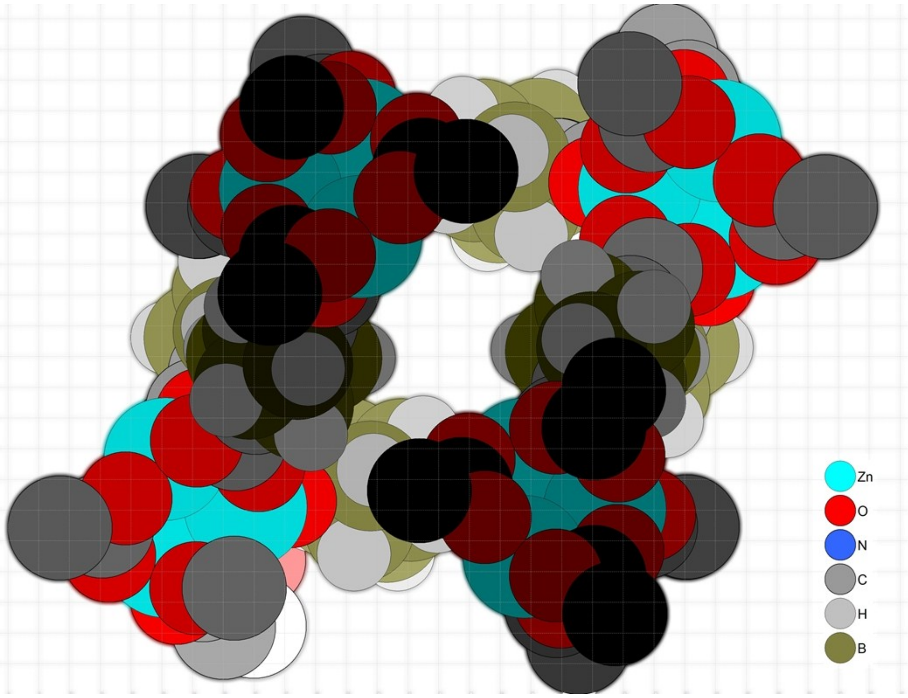

**SFig. 6.** Pore opening ( ~4×4 Å) profile in [$Zn_4OL_3(DEF)_3$], with solvent molecules removed. View along z-axis with angstrom grid overlay (1×1 Å mesh) and depth cueing (darker regions represents areas closer to the viewer).

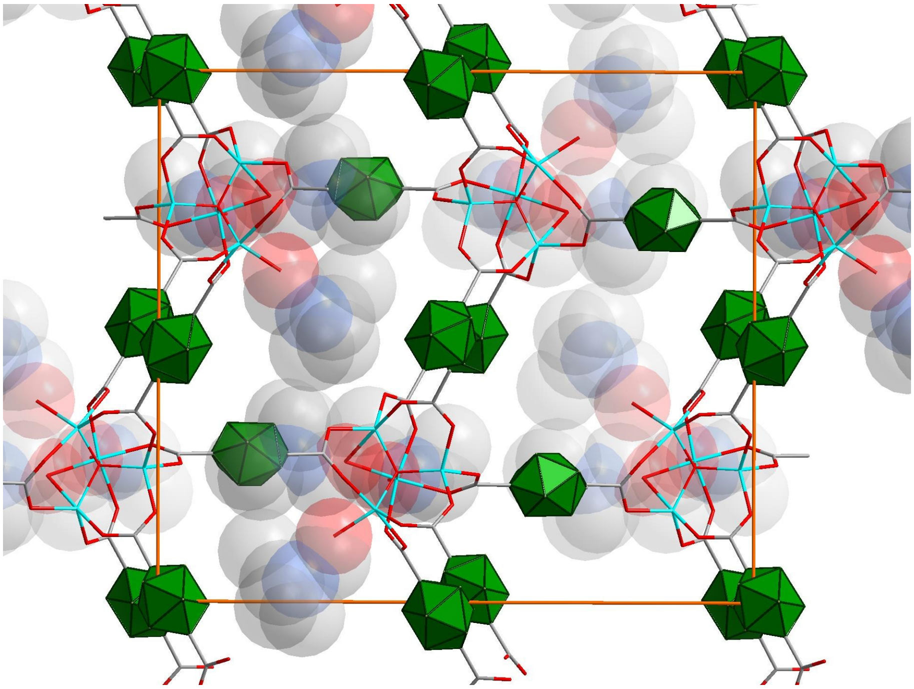

**SFig. 7.** The distribution of solvent molecules, shown half transparent (space filling model) in [$Zn_4OL_3(DEF)_3$].

The dense packing of solvent molecules shown on Fig. 7 explains the asymmetry in the distribution of the coordinated solvent molecules, (Fig. 5) as there is not enough space for hosting an additional, fourth solvent molecule coordinated to the {$Zn_4O(RCOO)_6$} cluster. That might imply that the change of the solvent's nature could change the result of the assembly, however no such proofs were obtained as of yet, by using also DMF and DMA based solvent mixtures.

## [Co(DMF)L], 2

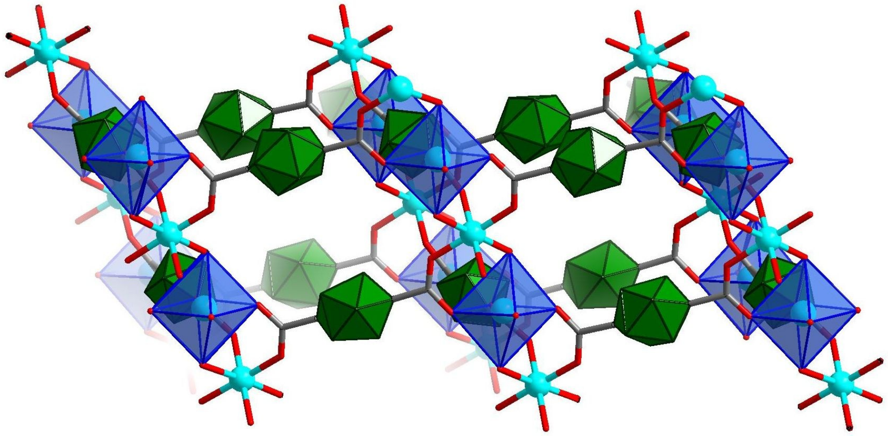

**SFig. 8.** Interpretation of the [Co(DMF)L] structure as having a topology equivalent to primitive cubic net (**pcu**).

As the coordination bonded cluster is infinite, a node interpretation is taken as one node per two cobalt atoms. Each node makes 4+2 connections to the neighbouring nodes through the carborane struts only and through bridging $COO^-$, $O(CNMe_2)$ functions respectively.

The figure illustrates a possible decomposition to such sub-elements with only half of the cobalt atoms taken as nodes (blue octahedra) and the second half (light blue spheres) regarded as simple connectors between two neighbouring nodes.

The figure shows the principal connectivity as rows of main nodes, representing an arrangement equivalent to three sets of mutually orthogonal rows, and straightforwardly identified as primitive cubic topology (**pcu**).

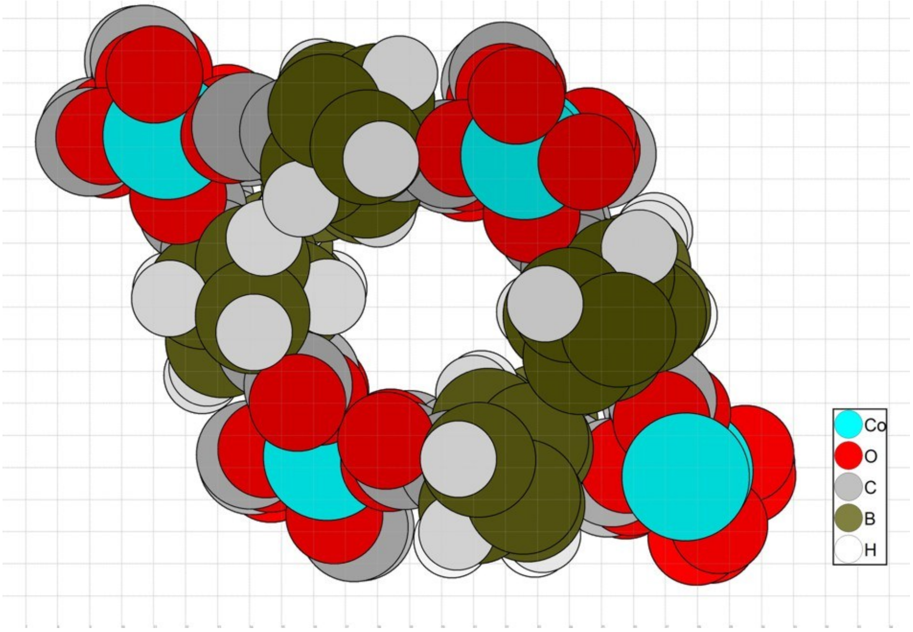

**SFig. 9.** Pore opening ( ~5×5 Å) profile in the structure of [Co(DMF)L] with the solvent molecules removed. View along x-axis with angstrom grid overlay and depth cueing.

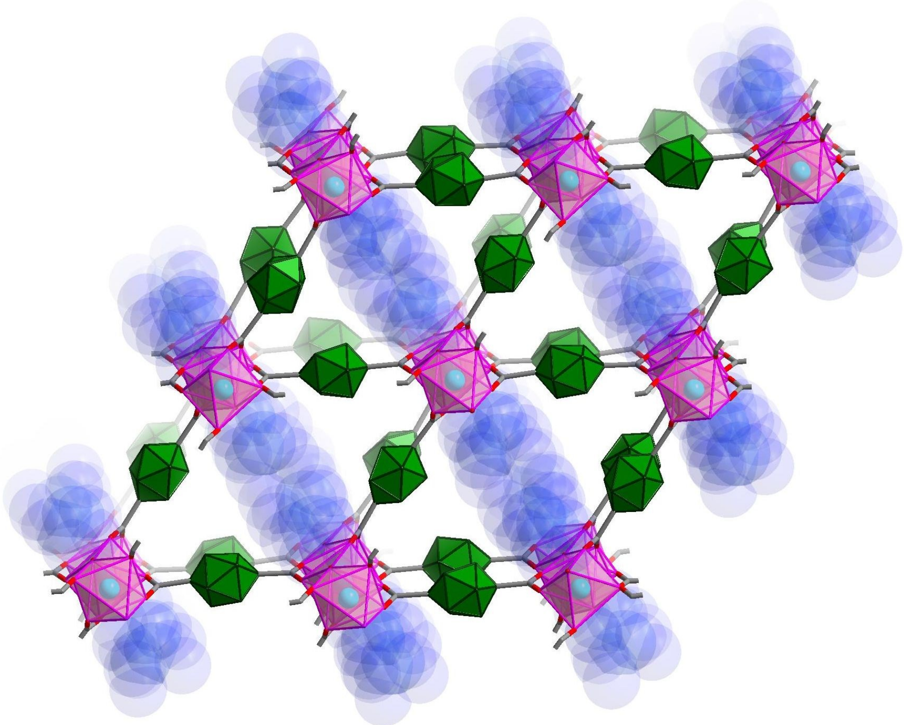

**SFig. 10.** The distribution of the disordered solvent molecules in the pores [Co(DMF)L]. The disordered parts of the DMF (i.e. except the coordinated oxygen atoms are given semitransparent, in space filling model, with slightly downscaled sizes for better visibility).

## $[Cu_2L_2(DMF)_2]$, 3

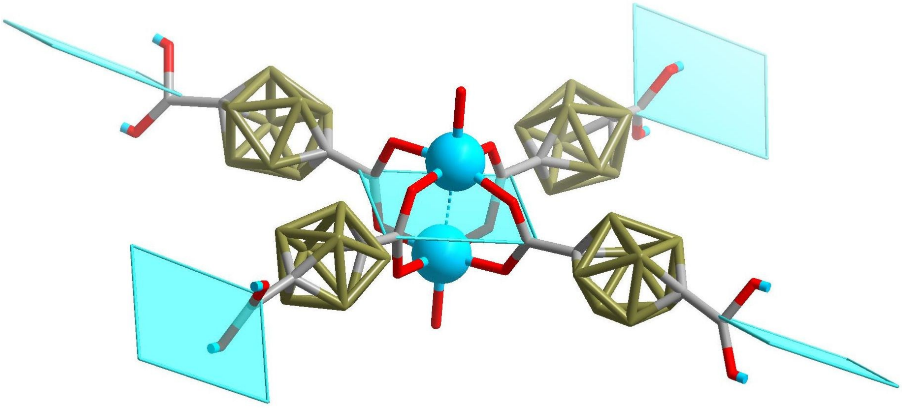

**SFig. 11.** The disposition of the neighbouring paddle-wheel unit in $[Cu_2L_2(DMF)_2] \cdot 2$ DMF (wire-frame model, the axial oxygen atom belongs to the coordinated solvent). The paddle-wheel's planes of symmetry are denoted as squares and the slight mutual turn, consisting of app. 20-25° is shown on the example of one of the five crystallographically independent units.

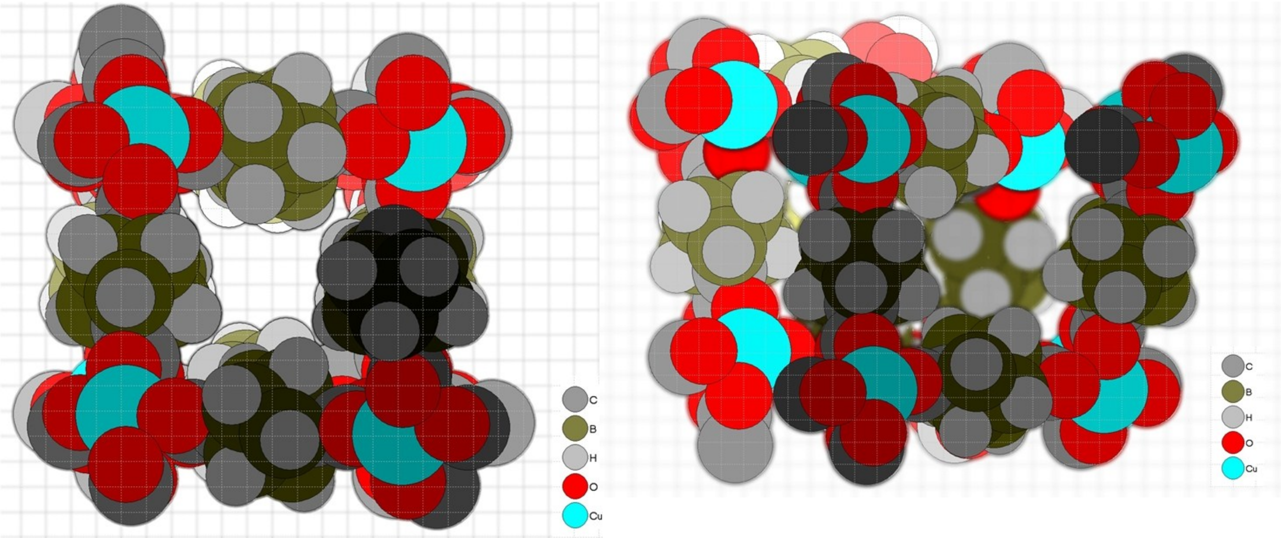

**SFig. 12.** Pore opening profile in $[Cu_2L_2(DMF)_2] \cdot 2$ DMF, with the solvent molecules removed. Angstrom grid overlay and depth cueing are applied and the distant in-depth regions are blurred for clarity.
View along x-axis on the left and a tilted view along the pore's undulating centerline (i.e. the set of points of maximum distance from the pore walls, or equivalently the set of centers of spheres of maximum diameter which could be placed in the pores) on the right. The pore's centerline is undulating, thus does not coinciding with the x-viewing direction and the pore width could be assessed as being at least 5×6 Å).

## *Adsorption measurements, experimental details*

Adsorption isotherms on the degassed samples, **1a** and **2a** were performed on a Micromeritics ASAP 2020 automatic gas sorption analyzer equipped with oil-free vacuum pumps (ultimate vacuum <$10^{-7}$ mbar) and valves, guaranteeing contamination free measurements.

A sequence of experiments aiming direct degassing (excluding solvent exchange) was performed on 20 to 50 mg samples of [$Zn_4OL_3(DEF)_3$], **1** and [Co(DMF)L], **2** (small amounts used are explained by choosing high quality small scale crystallization batches; this affected somewhat the precision, but as the samples were of significant porosity, even 10 mg of degassed sample was enough in order to surpass the recommended absolute surface area threshold for the ASAP 2020 instrument at 5 $m^2$). The samples, transferred quickly from storage-vials filled by argon, were quickly transferred in the measurement tubes, which were purged by dinitrogen gas, thus minimizing the time of contact with air. They were degassed / measured in a sequence of experiments, with step-by-step increasing temperature of degassing (180-350 °C) in order to find the optimal degassing conditions.

In a typical sequence, the samples were slowly and carefully degassed with evacuation rate 1 mmHg / s under heating rate of 0.5 °C/min up to ~100 °C and degassed at that temperature for additional 30 min. Then the temperature was allowed to increase to the target temperature in a 2 °C / min rate). The degassing at a constant target temperature continued until stabilization of the outgassing rate (the rate of pressure rise in the temporarily closed manifold with the connected sample tube, was less than 2 μTorr/min). After weighing, the sample tube was then transferred to the analysis port of the adsorption analyzer. Sequential experiments with different gases were performed on the same sample (the exceptions are reported in the summary Table S2), which was then subjected to a degassing at higher temperature with a step of app. 50 C and a new cycle of experiments.

All used gases ($H_2$, He, $N_2$, $CO_2$) were of ultra high purity (UHP, grade 5.0, 99.999% or of higher purity) and the STP volumes are given according to the NIST standards (293.15 K, 101.325 kPa). Helium gas was used for the determination of the cold and warm free space of the sample tubes. $H_2$ and $N_2$ adsorption isotherms were measured at 77 K (liquid nitrogen bath), and at 87K (liquid argon bath), whereas $CO_2$ adsorption isotherms were measured at temperatures ranged from 273 to 333K, controlled by high precision cryostat designed for adsorption measurement (E-lab services).

## [$Zn_4OL_3$], 1a

N$_2$ adsorption

**Table S2.** Summary table on adsorption measurement interpretations

| $T_{degas}$ | BET | | M-BET[1] | | | Langmuir | Δm |
|---|---|---|---|---|---|---|---|
| [°C] | $P/P_o$ = 0.01-0.12 | | | | | | |
| | S | C | S | C | Vμ | S | |
| | [$m^2$ $g^{-1}$] | | [$m^2$ $g^{-1}$] | | [$cm^3$ $g^{-1}$] | [$m^2$ $g^{-1}$] | [%] |
| 200 | 774 | -12957 | 101 | 19.3 | 0.277 | 927 | 31.9 |
| 200* | 794 | 5170 | 147 | 17.8 | 0.273 | 991 | 31.9 |
| 250 | 711 | 12672 | 101 | 13.9 | 0.256 | 873 | 32.0 |
| 180** | **896** | 24407 | 96 | 18.0 | 0.327 | 1062 | 32.0 |

* - degassed prior the measurement at 130°C for 2h,

** - a fresh sample, degassed at 180°C for 3.5day

[1] M-BET given for comparison, but the obtained values are meaningless, showing the non-applicability of the method in this case.

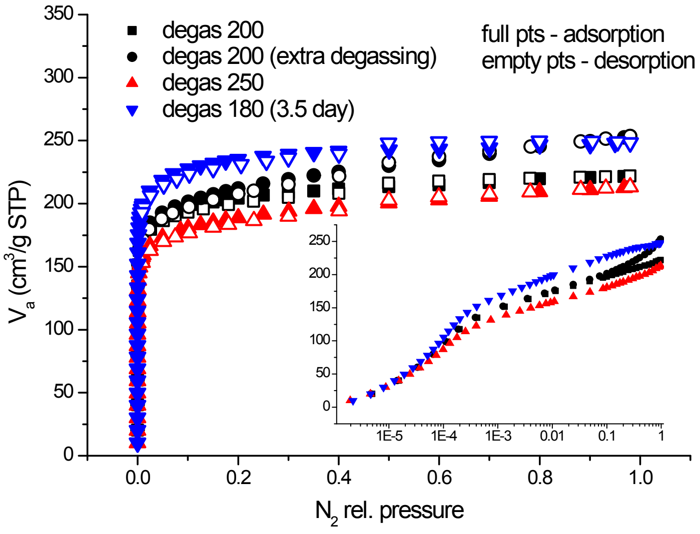

**SFig. 13.** $N_2$ adsorption isotherms for **1a** samples.

The initial [$Zn_4OL_3(DEF)_3$], **1** was degassed at different temperatures and the optimum porosity was reached at prolonged, 3.5 days long degassing at 180 °C. The low temperature optimum confirms the possible very slow framework-disintegrational processes suggested by TGA (Fig. 23, 24), which start below 200 °C.

## [CoL], 2a

### $N_2$ adsorption

**Table S3.** Summary table on adsorption measurement interpretations

| $T_{degas}$ [°C] | BET P/P$_o$ = 0.01-0.12 | | M-BET[1] | | | Langmuir | Δm |
|---|---|---|---|---|---|---|---|
| | S [m² g⁻¹] | C | S [m² g⁻¹] | C | Vµ [cm³ g⁻¹] | S [m² g⁻¹] | [%] |
| 250°C | 308 | -1943.8 | 21.58 | 17.27 | 0.115 | 356 | 21.0 |
| 300°C | **382** | -793.97 | 35.44 | 15.94 | 0.144 | 456 | 27.2 |
| 350°C | 280 | 2408 | 41.24 | 63.98 | 0.099 | 339 | 27.2 |

[1] M-BET, given for comparison, but the obtained values are meaningless, showing the non-applicability of the method in this case.

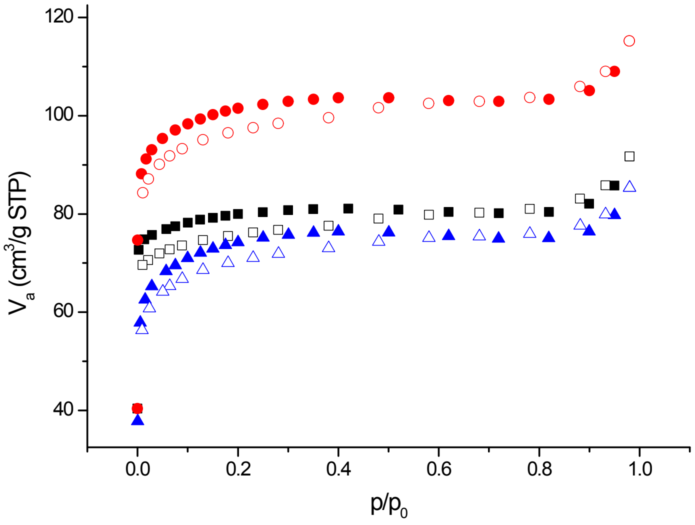

**SFig. 14.** $N_2$ adsorption isotherms for **2a** samples.
The initial [Co(DMF)L], **2** was degassed at different temperatures and the optimum porosity was reached at 250 °C (the colours correspond to degassing temperatures: blue - 250 °C, red - 300 °C, black - 350 °C).

## $CO_2$ adsorption

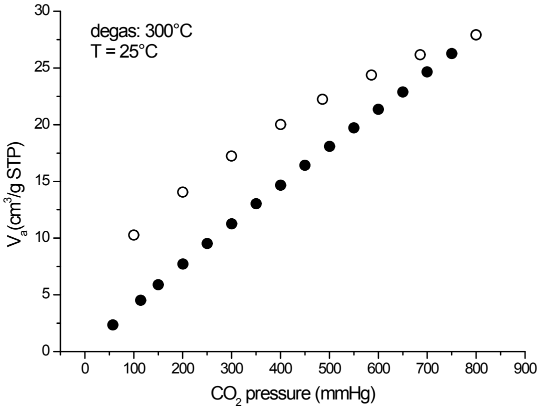

**SFig. 15.** $CO_2$ adsorption isotherms for **2a** after degassing at 300 °C. The hysteresis is not closed due to kinetic effects.

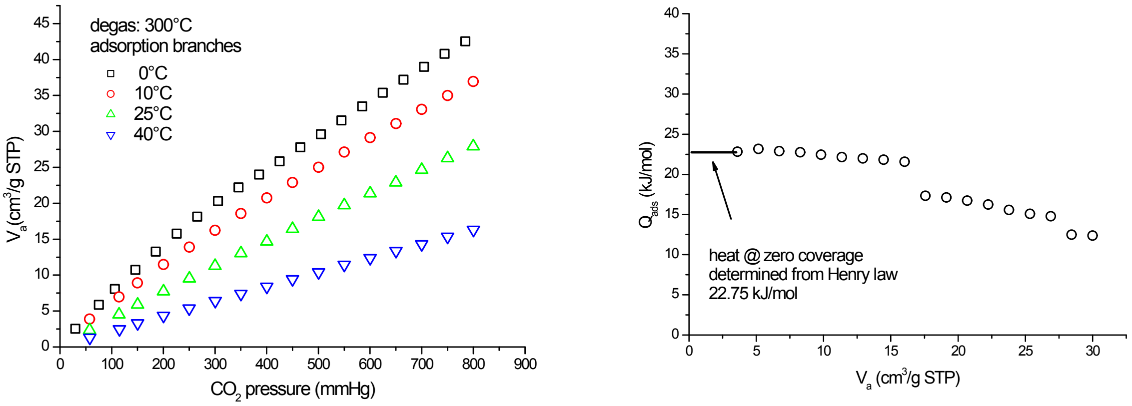

**SFig. 16**. CO2 adsorption isotherms at 0°C – 40°C (left) for [CoL] degased at 300°C and heat of adsorption (right) derived from Henry constants using the low pressure part of adsorption branch at various temperatures.

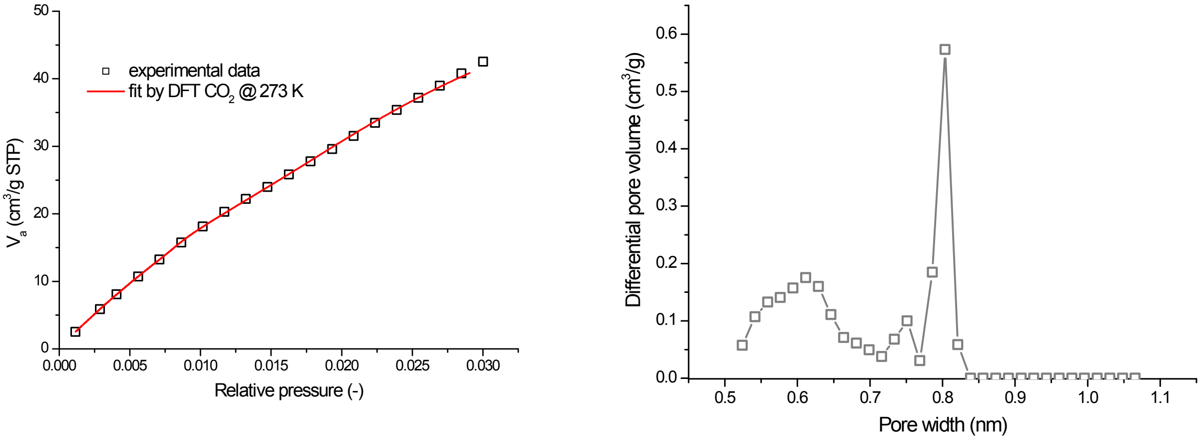

**SFig. 17.** Pore size distribution for **2a** after degassing at 300°C calculated by DFT CO$_2$ @ 273K model on carbon slit pores as implemented in the ASAP 2020 software.

## $H_2$ adsorption

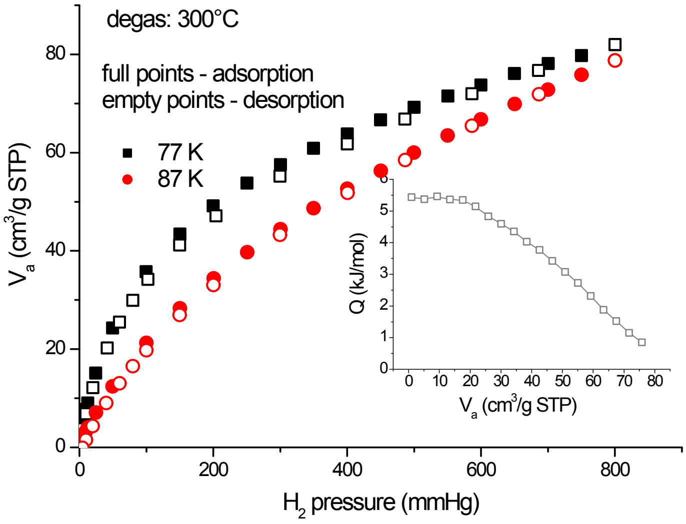

**SFig. 18.** $H_2$ adsorption isotherms at 77K (liquid $N_2$) and 87K (liquid Ar).
The volume absorbed at 800 mmHg and 77K was 81.96 cm$^3$/g (0.73 wt. %). Max. heat of adsorption at zero coverage is 5.4 kJ/mol.

## PXRD

The measurement was done using a Panalytical Xpert Pro powder diffractometer (Cu Kα source) in transmission mode. The isolated samples, which were stored under argon, were quickly ground in air and placed between two Kapton films, using a standard sample-holder, which precluded further contact with air (which was, most probably, a non-necessary precaution).

Below the superimposed - experimental and simulated from the single crystal diffraction - patterns are shown:

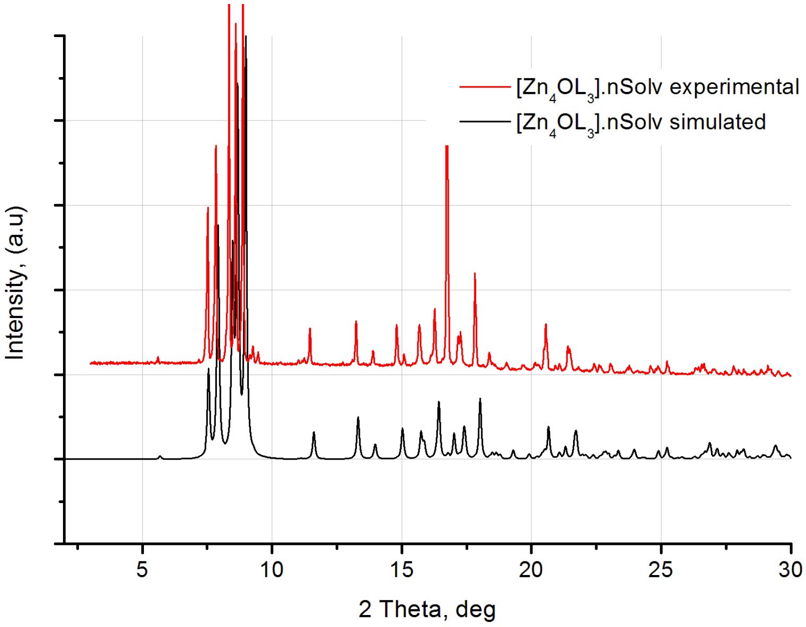

**SFig. 19.** Comparison of the simulated and experimental PXRD pattern for [$Zn_4OL_3(DEF)_3$].

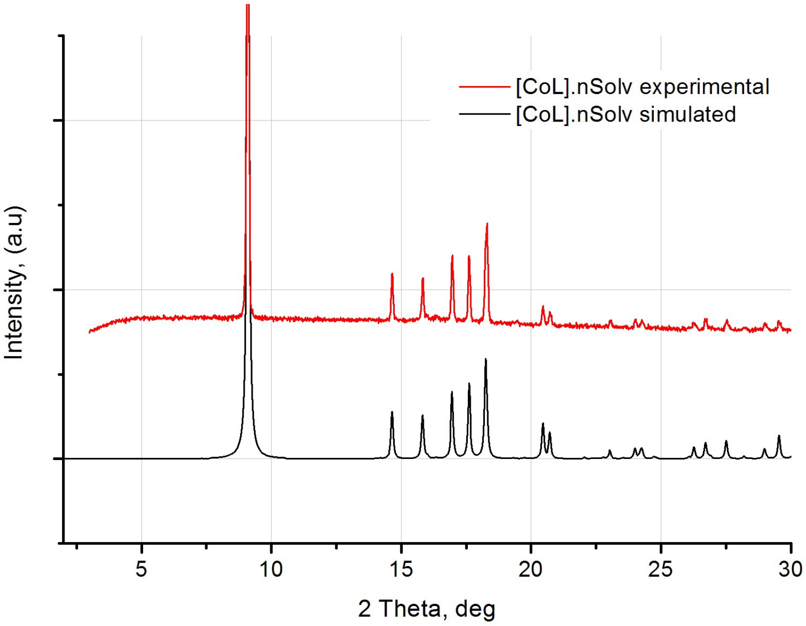

**SFig. 20.** Comparison of the simulated and experimental PXRD pattern for [Co(DMF)L], **1**

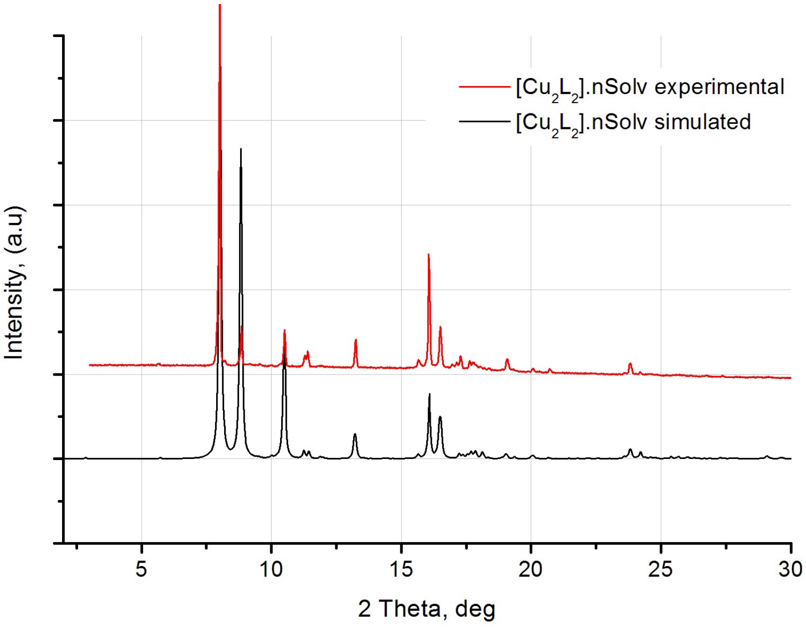

**SFig. 21.** Comparison of the simulated and experimental PXRD pattern for $[Cu_2L_2(DMF)_2] \cdot 2$ DMF

## TGA

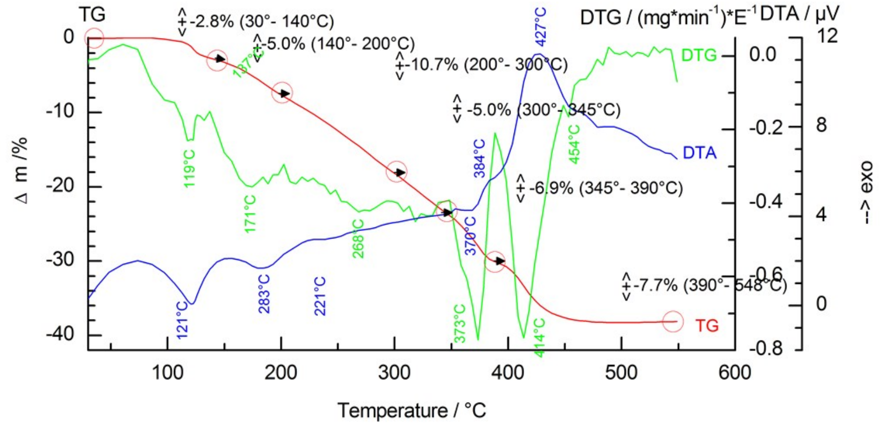

**SFig. 22.** TG-DTA of [Zn$_4$OL$_3$(DEF)$_3$], **1**.

Weight loss from r.t. to 350°C (see also SFig. 23) is 23.9% or 281 Da, which is slightly less than 3 molecules of DEF, which corroborates the structural data. The first small step of 2.8% or (35 Da) is clearly pertains to water, but it is, at least partially, a surface adsorbed amount, and it was not included in the final formula. Its presence is explained by the fact that the TG-DT analysis was performed on a sample which contacted with air for at least ≈ 15-30 min.

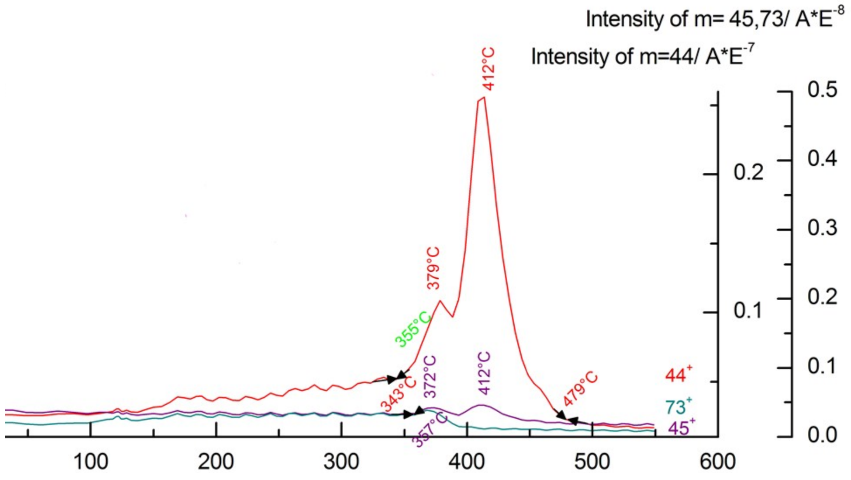

**SFig. 23.** MS spectra of the exhaust gas during TGA for [Zn$_4$OL$_3$(DEF)$_3$], **1**.

The molecular peaks, M$^{+\cdot}$ (electron ionization) carbon dioxide (44), $CH_3CH_2O^{+\cdot}$ (45; low intensity), diethylamine (73; low intensity).

The spectrum witnesses that:

- the framework is relatively stable to 350 °C, at which point the decarboxylation of the ligand speeds up rapidly (two waves are registered, at 379 °C and 420 °C).
- slow evolution of diethylamine originating from thermal decomposition of N,N-diethylformamide, which seemingly has low mobility in the pores, continues practically until 400 °C when it abruptly ceases, demonstrating complete disintegration of the framework.

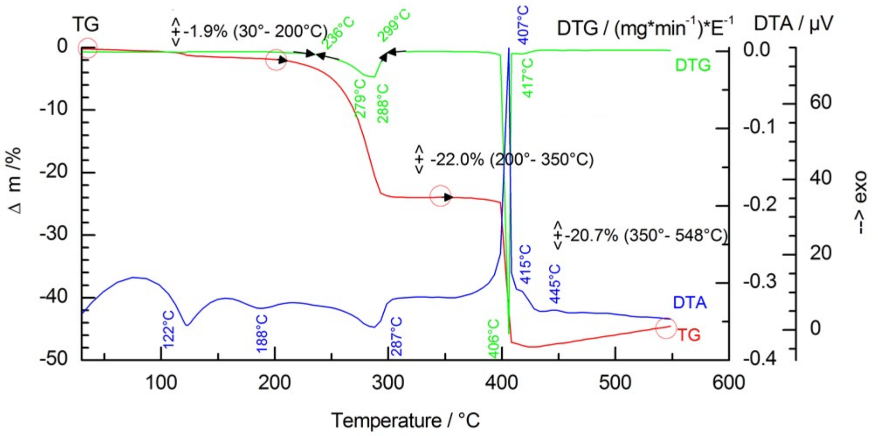

**SFig. 24.** TG-DTA of [Co(DMF)L], **2**.

The weight loss in the range of r.t. to 300 °C (see also SFig. 25) is 23.8% or 83 Da, which correspond approximately to 1 molecule of DMF. The actually observed weight loss is larger than the expected one due to contribution of a minor amount of surface adsorbed water and to the commencing deeper decomposition just prior 300 °C, which is concomitant with the loss of the last traces of the remarkably strongly bound DMF .

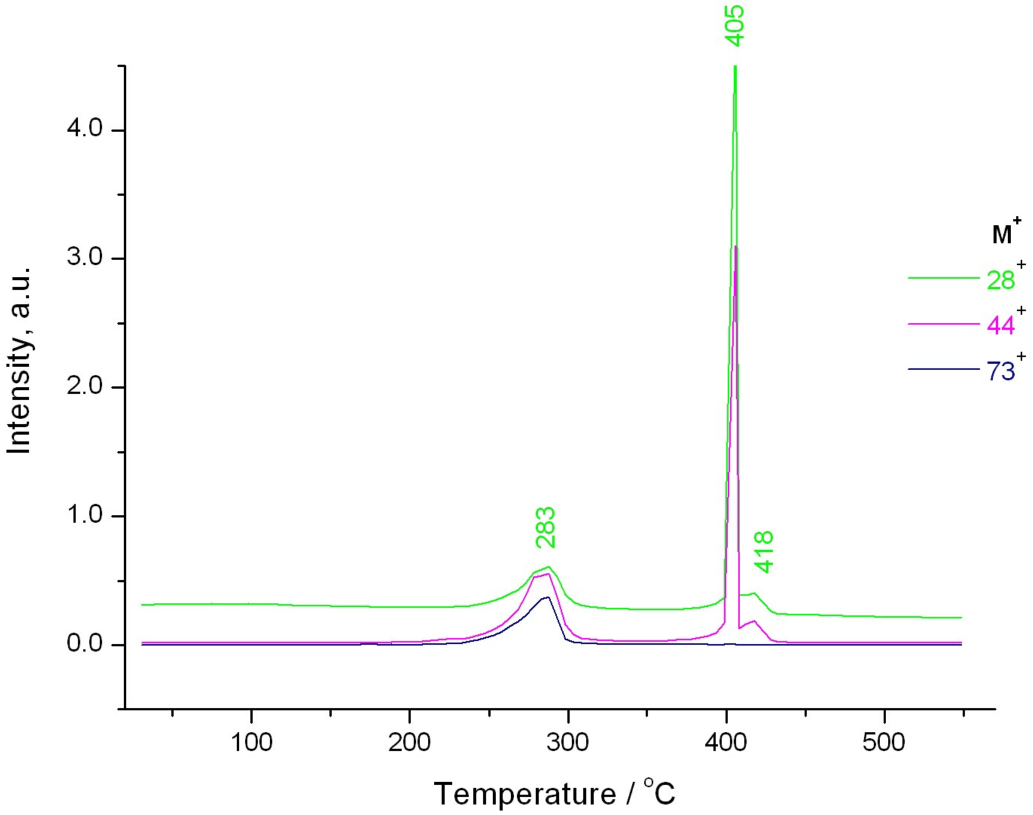

**SFig. 25.** MS spectra of the exhaust gas during TGA for [Co(DMF)L], **2**.

The molecular peaks, $M^{+\cdot}$ (electron ionization) associated with nitrogen or carbon monooxide gases (28), , carbon dioxide (44), DMF (73; low intensity).

According to the spectrum, the framework is relatively stable at least to 250 °C, but then some partial framework decomposition accompanied with decarboxylation and release of $CO_2$ occurs. Nevertheless, the major decarboxylation steps occurs rather at 400 °C with imminent complete collapse of the framework, which retains integrity at least partially up to this temperature.

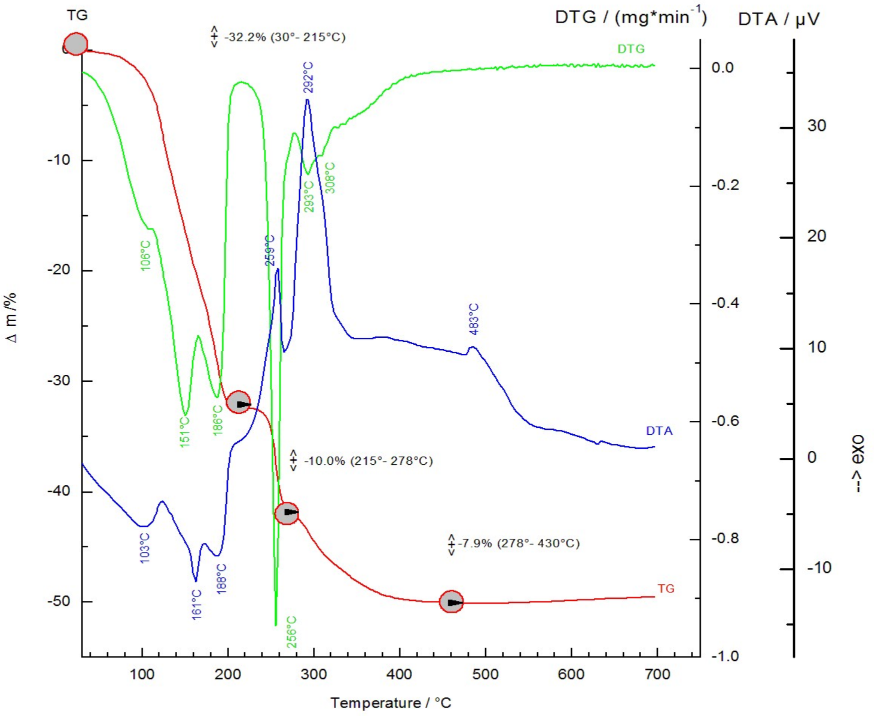

**SFig. 26.** TG-DTA of $[Cu_2L_2(DMF)_2] \cdot 2\ DMF$, **3**.

Weight loss from r.t. to 210 °C is 32.2 % or 257 Da, which correspond to somewhat less than 4 molecules of DMF (no MS data was collected, but according to our experience the copper carboxylate MOFs are prone to decarboxylate at relatively low temperature, i.e. the second weight-loss wave should be at least partially associated with the latter process (see also the exothermic character of the decarboxylative framework disintegration in the previous examples, which gives additional support for the same character of the process, which took place in the range of ≈210-280 °C).

The isolated compound might contain some minor amounts of water, but it is impossible to determine reliably the difference between the surface adsorbed water and the part, inherently residing in the pores. As the amount is relatively low (in any case could not be more than 1-2 molecules per formula unit), it is neglected for the sake of simplicity.

## *IR*

The samples were measured immediately after grinding, avoiding prolonged contact with air in nujol. The suspension was placed between KBr pellets and the measurement was carried out using a Nicolet Avatar 360 FTIR instrument. The Nujol characteristic bands are 3000-2850, 1465-1450, 1380-1370 cm$^{-1}$ (see also SFig. 30).

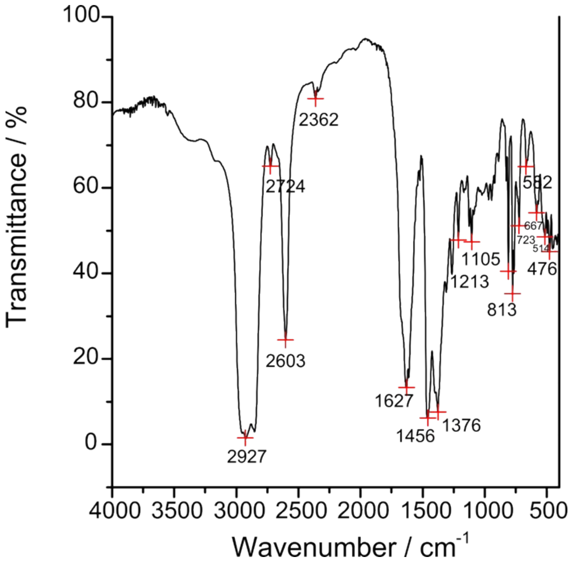

**SFig. 27.** IR spectrum of [$Zn_4OL_3(DEF)_3$], **1** (in Nujol).

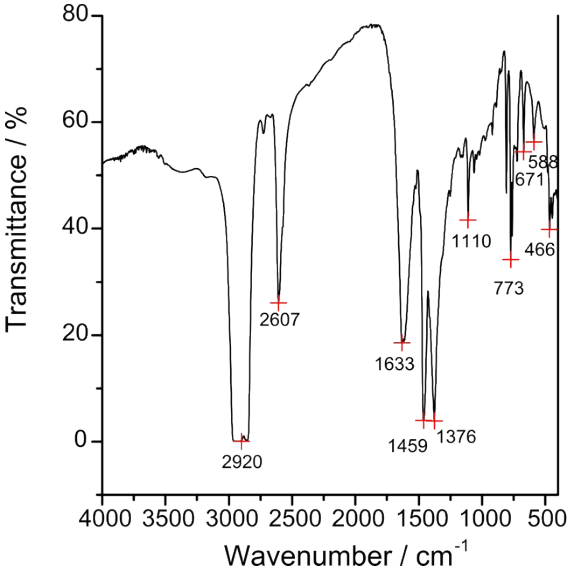

**SFig. 28.** IR spectrum of [Co(DMF)L], **2** (in nujol).

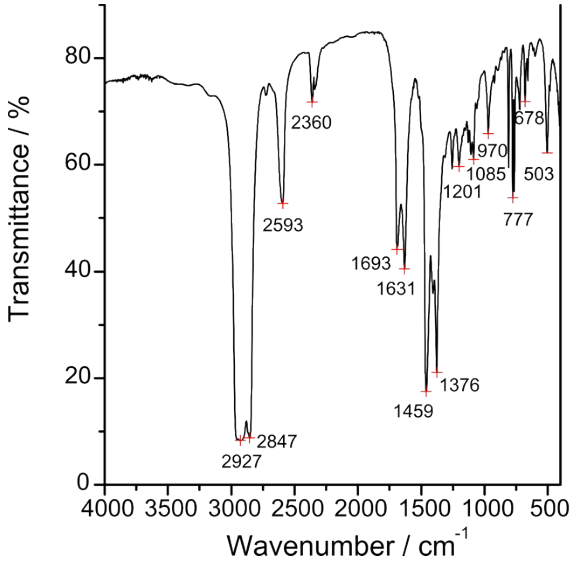

**SFig. 29.** IR spectrum of $[Cu_2L_2(DMF)_2] \cdot 2$ DMF, **3**(in nujol).

The residues after performing the TGA (700 °C) were also measured (the spectra are not shown, with an exception of a representative example of [Co(DMF)L]) and it was found that the absolute majority of carborane-characteristic BH stretching vibration bands (2590 - 2610 cm$^{-1}$) disappeared, which is consistent with sublimation of the boron containing residues, most probably in the form of the ligand's decarboxylation product, *closo*-1,10-dicarbadecaborane.

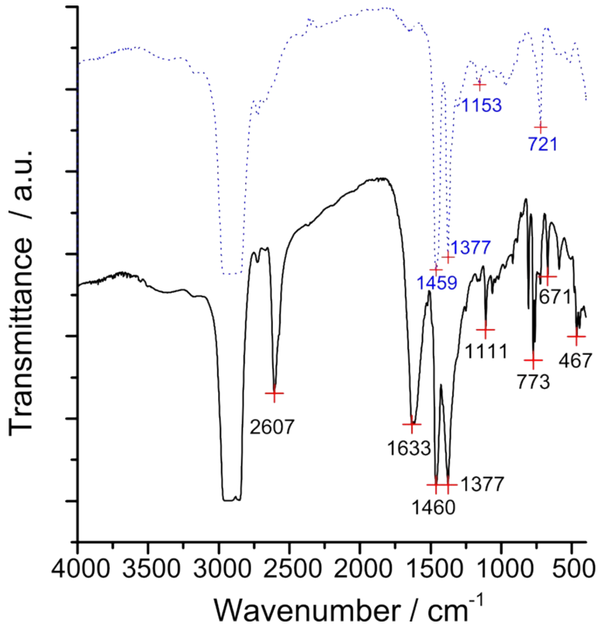

**SFig. 30.** Comparison of the IR spectra of [Co(DMF)L], **2** and the residues after TGA (both in nujol). Note the disappearance of the carborane-associated peak (2607 cm$^{-1}$) and the $\nu_{CO}$ peak of the DMF. The comparison also shows explicitly the nujol related adsorbance (2850-3000, 1460, 1377 cm$^{-1}$)

An other common feature is the presence of the $\nu_{as}$ band associated with C=O band in DMF 1635-1630 cm$^{-1}$ for the coordinated DMF molecules and 1693 cm$^{-1}$ for the non-coordinated ones (the same band in liquid DMF is at ≈1690-1670 cm$^{-1}$). The latter band, corresponding to 'free' DMF is observed only for $[Cu_2L_2(DMF)_2] \cdot 2\,DMF$, thus supporting the presence of non-coordinated DMF molecules, but not for the complexes of zinc and cobalt, which is concordant with the SC XRD data.

## *SEM*

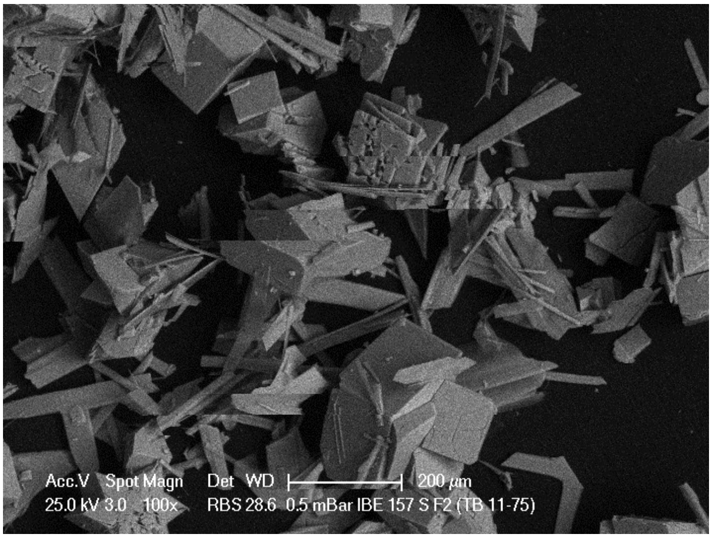

**SFig. 31.** Scanning electron micrograph of [$Zn_4OL_3(DEF)_3$], **1**.

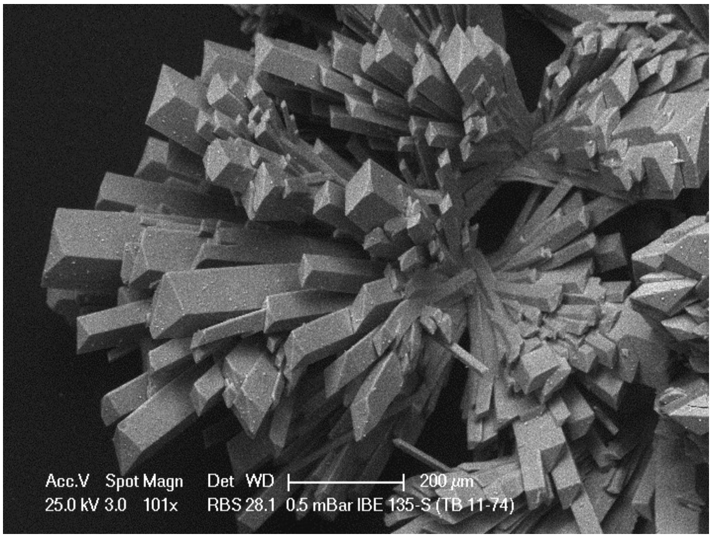

**SFig. 32.** Scanning electron micrograph of [Co(DMF)L], **2**.

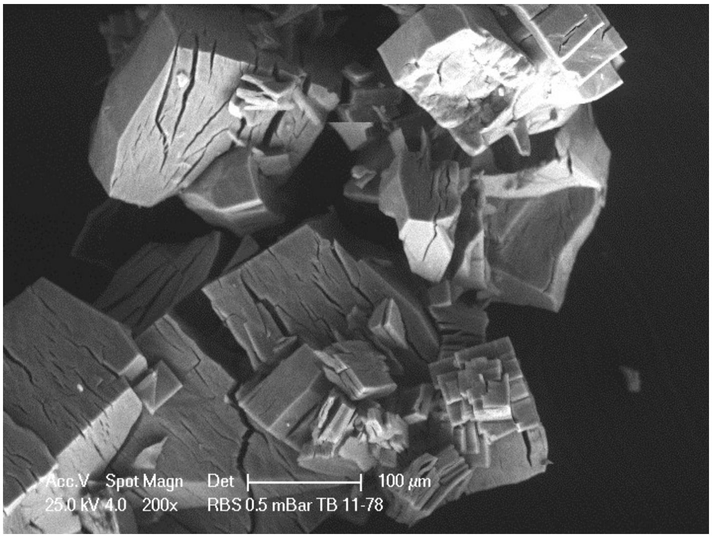

**SFig. 33.** Scanning electron micrograph of the pure [$Cu_2L_2(DMF)_2$] · 2 DMF, **3**

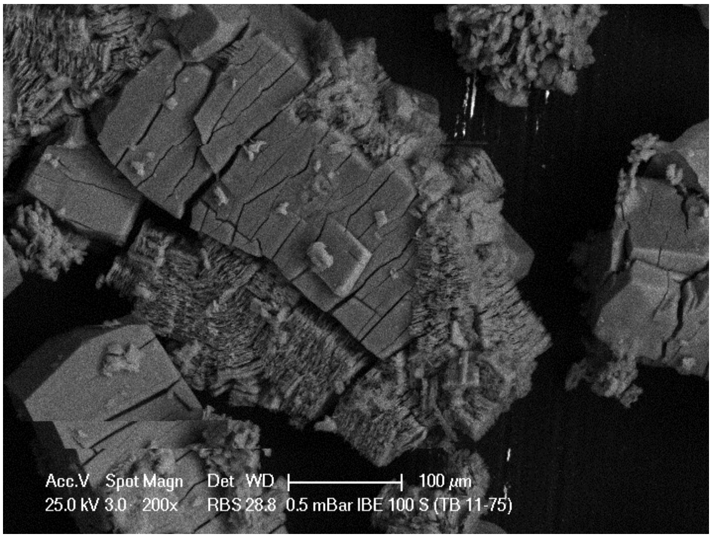

**SFig. 34.** Scanning electron micrograph of [$Cu_2L_2(DMF)_2$] · 2 DMF, **3**, with the concomitant laminar phase present

## Conformational analysis

The rotation profiles of the carboxyl group of 1-COO$^{(-)}$-1,12-*closo*-$C_2B_{10}H_{11}$ and 1-COO$^{(-)}$-1,10-*closo*-$C_2B_8H_9$ anions were calculated using the open-source quantum chemical package NWChem[1] as the reaction paths of the rearrangements from one extreme position of the carboxyl to another, determined by the NEB algorithm.[2,3] To compute the energies of the studied structures the DFT method was applied with the hybrid functional PBE0 [4,5] and Jensen polarisation consistent basis set pc-1.[6],[7],[8],[9]

In both cases one extreme was chosen as one carboxyl oxygen atom eclipsing the nearest cage boron (the respective torsion angle 0°). For the *closo*-decaborane skeleton, where the substituted carbon forms a square pyramid with the adjacent borons, it meant the other carboxyl oxygen eclipsing another cage boron, and the second extreme was set to the conformation with both oxygen atoms positioned above the middles of B–B edges of the carborane cage (torsion angle 45°). For the icosahedral *closo*-dodecaborane skeleton the substituted carbon forms an apex of a pentagonal pyramid, so that when one carboxyl oxygen eclipses the nearest boron atom (0°), the other oxygen points to the middle of the opposite B–B edge of the pentagon (36° torsion angle from its nearest boron neighbour). Thus the symmetrically unique arc of the carboxyl rotation ends at the torsion angle 18°, the other half of the arc to 36° being its mirror image.

---

[1] Valiev, M. *et al.* NWChem: A comprehensive and scalable open-source solution for large scale molecular simulations. *Comput. Phys. Commun.* **181,** 1477–1489 (2010).

[2] Henkelman, G., Uberuaga, B. P. & Jónsson, H. A climbing image nudged elastic band method for finding saddle points and minimum energy paths. *J. Chem. Phys.* **113,** 9901 (2000).

[3] Henkelman, G. & Jónsson, H. Improved tangent estimate in the nudged elastic band method for finding minimum energy paths and saddle points. *J. Chem. Phys.* **113,** 9978–9985 (2000).

[4] Adamo, C. & Barone, V. Toward reliable density functional methods without adjustable parameters: The PBE0 model. *J. Chem. Phys.* **110,** 6158 (1999).

[5] Adamo, C. & Barone, V. Physically motivated density functionals with improved performances: The modified Perdew–Burke–Ernzerhof model. *J. Chem. Phys.* **116,** 5933 (2002).

[6] Jensen, F. Polarization consistent basis sets: Principles. *J. Chem. Phys.* **115,** 9113 (2001).

[7] Jensen, F. Erratum: 'Polarization consistent basis sets: Principles' [J. Chem. Phys. 115, 9113 (2001)]. *J. Chem. Phys.* **116,** 3502 (2002).

[8] Jensen, F. Polarization consistent basis sets. II. Estimating the Kohn–Sham basis set limit. *J. Chem. Phys.* **116,** 7372 (2002).

[9] Jensen, F. Polarization Consistent Basis Sets. 4: The Elements He, Li, Be, B, Ne, Na, Mg, Al, and Ar †. *J. Phys. Chem. A* **111,** 11198–11204 (2007).

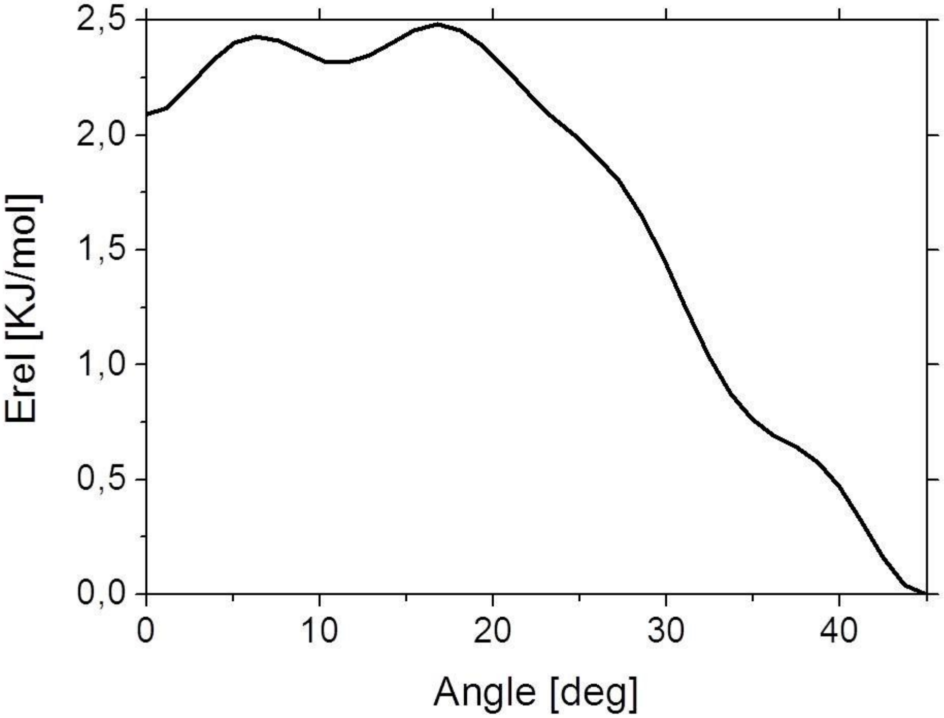

**SFig. 35.** Conformational analysis of 1-COO$^{(-)}$-1,10-*closo*-$C_2B_8H_9$ anion.

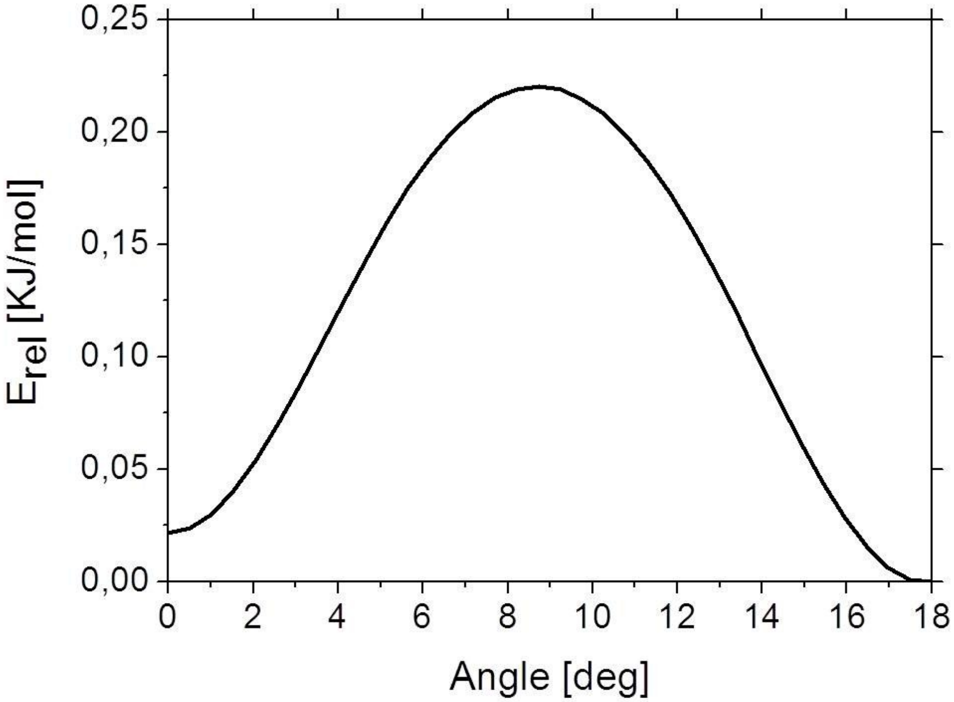

**SFig. 36.** Conformational analysis of 1-COO$^{(-)}$-1,12-*closo*-$C_2B_{10}H_{11}$ anion.

Tables with the computational data:

1-COO$^{(-)}$-1,10-$C_2B_8H_9$

| Angle[deg] | Energy[hartree] | $E_{rel}$[kJ/mol] | $E_{rel}$/RT | exp(-$E_{rel}$/RT) |
|---|---|---|---|---|
| -0,08 | -468,564090660514 | 2,0855 | 0,8361 | 0,4334 |
| 1,21 | -468,564077390457 | 2,1203 | 0,8501 | 0,4274 |
| 2,49 | -468,564042319547 | 2,2124 | 0,8870 | 0,4119 |
| 3,77 | -468,564001116611 | 2,3206 | 0,9303 | 0,3944 |
| 5,06 | -468,563970803697 | 2,4002 | 0,9622 | 0,3820 |
| 6,35 | -468,563960252370 | 2,4279 | 0,9733 | 0,3778 |
| 7,64 | -468,563967373291 | 2,4092 | 0,9659 | 0,3807 |
| 8,93 | -468,563984822223 | 2,3634 | 0,9475 | 0,3877 |
| 10,23 | -468,563999996114 | 2,3235 | 0,9315 | 0,3940 |
| 11,54 | -468,564002845586 | 2,3160 | 0,9285 | 0,3951 |
| 12,84 | -468,563991419880 | 2,3460 | 0,9405 | 0,3904 |
| 14,14 | -468,563970151011 | 2,4019 | 0,9629 | 0,3818 |
| 15,45 | -468,563949133456 | 2,4571 | 0,9851 | 0,3734 |
| 16,76 | -468,563939616565 | 2,4820 | 0,9951 | 0,3697 |
| 18,08 | -468,563949950781 | 2,4549 | 0,9842 | 0,3737 |
| 19,40 | -468,563975436503 | 2,3880 | 0,9574 | 0,3839 |
| 20,71 | -468,564013492505 | 2,2881 | 0,9173 | 0,3996 |

| | | | | |
|---|---|---|---|---|
| 22,02 | -468,564054135410 | 2,1814 | 0,8745 | 0,4171 |
| 23,33 | -468,564091069435 | 2,0844 | 0,8357 | 0,4336 |
| 24,63 | -468,564122418777 | 2,0021 | 0,8027 | 0,4481 |
| 25,94 | -468,564157511645 | 1,9100 | 0,7657 | 0,4650 |
| 27,24 | -468,564198897211 | 1,8013 | 0,7222 | 0,4857 |
| 28,55 | -468,564256405211 | 1,6503 | 0,6616 | 0,5160 |
| 29,85 | -468,564330121663 | 1,4568 | 0,5840 | 0,5576 |
| 31,14 | -468,564411839442 | 1,2422 | 0,4980 | 0,6077 |
| 32,42 | -468,564489180783 | 1,0392 | 0,4166 | 0,6593 |
| 33,68 | -468,564552286862 | 0,8735 | 0,3502 | 0,7046 |
| 34,94 | -468,564594652063 | 0,7622 | 0,3056 | 0,7367 |
| 36,19 | -468,564620466236 | 0,6945 | 0,2784 | 0,7570 |
| 37,45 | -468,564639848020 | 0,6436 | 0,2580 | 0,7726 |
| 38,72 | -468,564665774347 | 0,5755 | 0,2307 | 0,7940 |
| 39,98 | -468,564706655225 | 0,4682 | 0,1877 | 0,8289 |
| 41,24 | -468,564762776954 | 0,3208 | 0,1286 | 0,8793 |
| 42,49 | -468,564823691812 | 0,1609 | 0,0645 | 0,9375 |
| 43,71 | -468,564869936500 | 0,0395 | 0,0158 | 0,9843 |
| 44,94 | -468,564884976538 | 0,0000 | 0,0000 | 1,0000 |

1-COO$^{(-)}$-1,12-$C_2B_{10}H_{11}$

| Angle[deg] | Energy[hartree] | $E_{rel}$[kJ/mol] | $E_{rel}$/RT | exp(-$E_{rel}$/RT) |
|---|---|---|---|---|
| 0,00 | -519,452369182331 | 0,0217 | 0,0087 | 0,9913 |
| 0,51 | -519,452368407496 | 0,0238 | 0,0095 | 0,9905 |
| 1,03 | -519,452365951701 | 0,0302 | 0,0121 | 0,9880 |
| 1,54 | -519,452362055948 | 0,0404 | 0,0162 | 0,9839 |
| 2,06 | -519,452356940974 | 0,0539 | 0,0216 | 0,9786 |
| 2,57 | -519,452350933369 | 0,0696 | 0,0279 | 0,9725 |
| 3,09 | -519,452344315164 | 0,0870 | 0,0349 | 0,9657 |
| 3,60 | -519,452337256527 | 0,1055 | 0,0423 | 0,9586 |
| 4,11 | -519,452330158622 | 0,1242 | 0,0498 | 0,9514 |
| 4,63 | -519,452323248013 | 0,1423 | 0,0571 | 0,9445 |
| 5,14 | -519,452316734103 | 0,1594 | 0,0639 | 0,9381 |
| 5,65 | -519,452310807319 | 0,1750 | 0,0702 | 0,9323 |
| 6,17 | -519,452305565044 | 0,1887 | 0,0757 | 0,9271 |
| 6,68 | -519,452301325503 | 0,1999 | 0,0801 | 0,9230 |
| 7,19 | -519,452297949430 | 0,2087 | 0,0837 | 0,9197 |
| 7,71 | -519,452295498054 | 0,2152 | 0,0863 | 0,9173 |
| 8,22 | -519,452293985866 | 0,2191 | 0,0879 | 0,9159 |
| 8,73 | -519,452293541066 | 0,2203 | 0,0883 | 0,9155 |
| 9,25 | -519,452294100545 | 0,2188 | 0,0877 | 0,9160 |
| 9,76 | -519,452295706186 | 0,2146 | 0,0860 | 0,9176 |
| 10,28 | -519,452298322328 | 0,2078 | 0,0833 | 0,9201 |
| 10,80 | -519,452301901450 | 0,1984 | 0,0795 | 0,9236 |

| | | | | |
|---|---|---|---|---|
| 11,31 | -519,452306460706 | 0,1864 | 0,0747 | 0,9280 |
| 11,83 | -519,452311822413 | 0,1723 | 0,0691 | 0,9332 |
| 12,34 | -519,452317887763 | 0,1564 | 0,0627 | 0,9392 |
| 12,86 | -519,452324562889 | 0,1389 | 0,0557 | 0,9458 |
| 13,37 | -519,452331748870 | 0,1200 | 0,0481 | 0,9530 |
| 13,89 | -519,452339225706 | 0,1004 | 0,0402 | 0,9606 |
| 14,40 | -519,452346677236 | 0,0808 | 0,0324 | 0,9681 |
| 14,92 | -519,452353938134 | 0,0617 | 0,0248 | 0,9756 |
| 15,43 | -519,452360669557 | 0,0441 | 0,0177 | 0,9825 |
| 15,94 | -519,452366609159 | 0,0285 | 0,0114 | 0,9886 |
| 16,46 | -519,452371510991 | 0,0156 | 0,0063 | 0,9938 |
| 16,97 | -519,452375060621 | 0,0063 | 0,0025 | 0,9975 |
| 17,49 | -519,452377146361 | 0,0008 | 0,0003 | 0,9997 |
| 18,00 | -519,452377455218 | 0,0000 | 0,0000 | 1,0000 |